NUMERICAL ANALYSIS OF IMPURITIES DEPENDENCE OF THE TEMPERATURE FREEZING OF ZINC

Denise das Mercês Camarano
Instituto Nacional de Metrologia, Normalização e Qualidade Industrial – Universidade Federal de MG
Rua Jacuí, 3921, Bairro Ipiranga – 31 160 190 – Belo Horizonte - MG
dmcamarano@inmetro.gov.br

Vinícius Sena Moreira
Universidade Federal de Minas Gerais -UFMG
Av. Antônio Carlos, 6627- Bairro Pampulha - 31 210 901 – Belo Horizonte – MG
vsmor@yahoo.com.br

Roberto Márcio de Andrade
Universidade Federal de Minas Gerais – UFMG
Av. Antônio Carlos, 6627- Bairro Pampulha - 31 210 901 – Belo Horizonte – MG
rma@ufmg.br

Abstract. *A study of the liquid-solid transformation zinc point temperature have been made. Usually, the influence of impurities on the fixed-point temperature causes the main uncertainty component. In this paper we analyse numerically the effect of freezing rate at freezing point temperature of zinc with different impurity contents. The behavior of systems with a low value of equilibrium partition ratio was compared to other systems having diferent equilibrium partition ratio values .Results show that the overall shape of freezing curves is not appreciably altered by an increase in solute concentration. Estimated freezing ranges of the individual sample are in good agreement with the published experimental data.*

Keywords*: Temperature, freezing point of zinc, numerical simulation.*

1. Introduction

The freezing zinc point (697,277 K) has been used for many years as a fixed point on International Temperature Scale of 1990, ITS-90 (BIPM, 1990). In view of a lack of sufficient data on the behavior of impurities in the ITS-90 defining fixed point materials, for the assessment of the quality of fixed point realizations at the highest levels of accuracy, it is crucial to analyse in detail the influence of the concentrations of the material's impurities using different freezing conditions. There are two ways on which theoretical analysis may be attempted. The first one is by inspecting phase diagrams at extreme dilution (near 1 ppm impurity). Phase diagrams are usually extrapoleted to the origin from experimentals points many degrees away from the freezing temperature of pure material and with concentration greater than 1 % (Connoloy and McAllan, 1980). However, the lack of this knowledge has reduced the utility of impurity analyses in predicting behaviour. The second is calculation from the cryoscopic constant of the impurity material. However, cryoscopic calculations cannot predict the effect of a number of impurities in combinations, but only the binary contributions, and their sum. The information required for those calculations is analysis, which may or may not be a available, for various impurities of a particular metal (Sostemann,1993). A simple analysis of the melting or freezing curves, assuming incorrectly that the impurities are not soluble in the solid phase of the fixed point material and neglecting the effect of the freezing conditions, yields usually a significant underestimation of the influence of impurities on the temperature of the solid-liquid interface. In some cases, details of the history of the sample before it enters the phase transition, such as length of time in the liquid state before beginning the freeze, may be also important (BIPM,1999a and b).Some years ago a considerable amount of work was carried out with resistance thermometers on the freezing points of metals in the range of 0 ºC to 630 ºC under a variety of cooling and heating rates rates (McLaren 1958, 1962 and 1963; Connoly and McAllan,1975). Due to high cost of experiment only recently Ancsin (2003 and 2001) made a systematic study of shifts of equilibrium melting curves of samples Al and Ag. State-of-art estimates for the uncertainty component caused by impurities has been deduced from results obtained in the CIPM Key Comparions. However, no theoretical analysis or analysis of reported impurities in the bulk metal can completely assure the quality of a freeze point cell. Since it is not possible to obtain a reliable estimate for this influence from tha shape of the melting and freezing curves more expensive methods must be apllied. Thus, mathematical modelling becomes more attractive for exploring novel processing schemes. Numerical simulation based on valid mathematical models offers opportunities to gain insights into various physical phenomena that are difficult, if not impossible, to carry out experiments.

In recent years, much time and effort has been expended trying to develop accurate models, as well as efficient numerical algorithms to solve the governing equations related to transport phenomena that occur during alloy solidification. The aim of this paper is illustrating the use of the mathematical model to simulate the freezing point of zinc in order to better evaluate and understand the effects of impurities on fixed point temperature. Observations were

made to determine actual solute distributions and the relative freezing ranges of zinc point. In addition, the results may be compared to the results observed by Weinberg and McLaren (1963) and McLaren (1958).

2. Model description

In order to study possible solidification behaviors of zinc point, four numerical simulations were performed:

- the solidification of sample of CPZinc, SPZinc and Zn-Tl (20 ppm) takes place under freezing rate at about 0,02 K/s;
- for sample of Zn-Tl (8 ppm) the temperature changes in the melt before transformation under freezing rate at about 0,02 K/s after solidification proceeds freely.

In all simulations presented in this article the initial temperature were 5 K higher than the liquidus temperature and initial composition of elements is specified in Tab.1. A system (Zn-Tl) was selected to study the effect of freezing rate on the solute distribution because it has a low distribution coefficient (0,01) where segregation effects would be most pronounced and the phase diagram is known at low solute concentrations.

Table 1. Impurity content of CPZinc, SP Zinc and Zn-Tl

Impurity	CPZinc	SPZinc	Zn-Tl
Cd	0,000 05	0,000 05	-
Fe	0,000 4	-	-
Cu	0,000 05	-	-
Tl	-	-	0,000 006
Tl	-	-	0,000 020

The simulated geometry is shown in Fig. 1. The size was selected to be representative of a laboratory cell where the melt is placed in a cylindrical graphite crucible; a hole in a removable graphite top allows a graphite thermometer to be axially located in the melt. The cell's symmetry allows ¼ section of the geometry to be modelled. The top, bottom and the right wall of cell's geometry are insulated while a constant temperature is prescribed at the left wall. All walls are treated with no-slip condition and are impermeable to mass and species transport. The thermopysical properties and phase-diagram parameters are summarized in Tab.2. The interfacial length scale is assumed equal to 4 μm and difffusion lenghts for all species are assumed equal 1 μm. These parameters are constants and assumed to be representantive of those found in literature for zinc point. The melt is initially isothermal and chemically homogeneous.

Table 2.Thermophysical properties and phase-diagram parameters

Symbol	Properties	Value	Reference
L	Fusion enthalpy Zn (kJ/kg)	100,9	(ILZR, 1991)
T_f	Fusion temperature (K)	692,677	(BIPM,1990)
c_p	Liquid specific heat Zn (cal $g^{-1}\cdot$ ºC^{-1})	0,118	(McLaren and Murdock, VIIIb. 1968)
	Solid specific heat Zn (cal $g^{-1}\cdot$ ºC^{-1})	0,108	
K	Liquid thermal conductivity Zn (W cm^{-1} ºC^{-1})	0,60	
	Solid thermal conductivity Zn (W cm^{-1} ºC^{-1})	1,00	
P	Liquid density Zn (g cm^{-3})	6,6	
	Solid density Zn (g cm^{-3})	6,8	
β_T	Coefficient of thermal expansion Zn (K^{-1})	2,6 x 10^{-5}	(Brady *et al*., 1991)
μ	Liquid viscosity Zn (N $\cdot$ m^{-1})	0,003 85	(ILZR, 1991)
β_c	Solid coefficient of solutal expansion Cd, Fe and Tl (1/ wt pct)	-2	Assumed
	Liquid coefficient of solutal expansion Cu (1/ wt pct)	-5,48 x 10^{-4}	(Schneider, 1995)
D	Liquid mass coefficient difussion Cd, Fe and Tl (cm^2 s^{-1})	5 x 10^{-5}	(Campos *et al*.,1972)
	Liquid mass coefficient difussion Cu (cm^2 s^{-1})	2 x 10^{-9}	(Schneider, 1995)
	Solid mass coefficient difussion Cd, Fe and Tl(cm^2 s^{-1})	1 x 10^{-8}	(Campos *et al*.,1972)
	Solid mass coefficient difussion Cu (cm^2 s^{-1})	4,4 x 10^{-12}	(Schneider,1995)
K^n	Equilibrium partition ratio Zn-Cu	2,5	(Sotsmann,1993)
	Equilibrium partition ratio Zn-Cd	0,02	
	Equilibrium partition ratio Zn-Fe	0,12	
	Equilibrium partition ratio Zn-Tl	0,01	
m	Slope of the liquidus line Zn-Cu (10^{-4} ºC/ppm)	1,5	
	Slope of the liquidus line Zn-Cd (10^{-4} ºC/ppm)	-1,9	
	Slope of the liquidus line Zn-Fe (10^{-4} ºC/ppm)	-4,1	
	Slope of the liquidus line Zn-Tl (10^{-4} ºC/ppm)	-1,9	

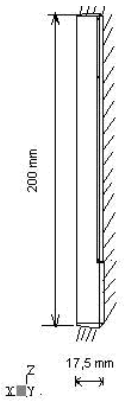

Figure 1. Geometry of cell zinc point

2.1. Mathematical formulation

Numerous models have been developed for the solidification alloys, and comprehensive reviews have recently been published (Ilegbus and Mat, 2000). In this study, the physical behavior of the solidification process is modeled through the use of a two-phase system of equations proposed by Ni and Beckermann (1991). Two sets of conservation equations are derived, one based on the liquid phase and one based on the solid phase. The continuity, momentum, energy, and species equations are expressed as

Continuity

$$\frac{\partial}{\partial t}\left(r_\alpha \rho_\alpha\right)+\nabla\cdot\left(r_\alpha \rho_\alpha U_\alpha\right)=\dot{m}_{\alpha\beta}A_{\alpha\beta} \tag{1}$$

where $\dot{m}_{\alpha\beta}$ is the mass flow rate per unit interfacial area $A_{\alpha\beta}$ from phase β to phase α. The volume fraction of α is denoted r_α.

Momentum

$$\frac{\partial}{\partial t}\left(r_\alpha \rho_\alpha U_\alpha\right)+\nabla\cdot\left(r_\alpha\left(\rho_\alpha U_\alpha\otimes U_\alpha\right)\right)=-r_\alpha\nabla p_\alpha+\nabla\cdot\left(r_\alpha\mu_\alpha\left(\nabla U_\alpha+\left(\nabla U_\alpha\right)^T\right)\right)+\sum_{\beta=1}^{N_p}\left(\Gamma^+_{\alpha\beta}U_\beta-\Gamma^+_{\beta\alpha}U_\alpha\right)+S_{MS\alpha} \tag{2}$$

where

$S_{M\alpha}$ ...describes momentum source term

$\left(\Gamma^+_{\alpha\beta}U_\beta-\Gamma^+_{\beta\alpha}U_\alpha\right)$ ... represents momentum transfer induced by interphase mass transfer.

The source term is expressed by:

$$S_M=\rho g[\beta_T(T-T_{ref})+\beta_c(C_l^n-C_{ref}^n)] \tag{3}$$

where g is gravitational accelaration, T is the casting melt temperature and C is the concentration (mass fraction). The subscript ref represents initial condition, the subscript l represents liquid phase and the superscript n represents species.

The modeling of the term of interphase mass transfer requires experimentals results of microstutural parameters. Flow through a muschy zone consisting of a continuous solid structure such as columnar dentritic crystals is usually very slow due to the high value of the interfacial area concentration. Therefore, the dissipative interfacial stress may be modeled approximately by Darcy's law. The term of interphase mass transfer is then modelled an linear source of resistance (C_{R1}) as:

$$C_{R1}=\frac{\mu}{K}. \tag{4}$$

A simple Blake-Cozeny expression is used to calculate the permeability function, K. Assuming the permeability to be isotropic:

$$K=K_o\left(\frac{r_\beta^3}{(1-r_\beta)^2}\right). \tag{5}$$

The value of K_o will pend on the morphology of the porous media. In the current study K_o is assumed constant and is of the order of 10^3.

Energy

$$\frac{\partial}{\partial t}\left(r_\alpha \rho_\alpha\right)+\nabla\cdot\left(r_\alpha\left(\rho_\alpha h_\alpha-\lambda_\alpha\nabla T_\alpha\right)\right)=\sum_{\beta=1}^{N_p}\left(\Gamma^+_{\alpha\beta}h_{\beta s}-\Gamma^+_{\beta\alpha}h_{\alpha s}\right)+Q_\alpha \tag{6}$$

where h_α, T_α, and λ_α denote the sensible enthalpy, temperature and the thermal conductivity of phase α. Q_α denotes interphase heat transfer to phase α across interfaces with other phases and ($\Gamma^+_{\alpha\beta}h_{\beta s}$ - $\Gamma^+_{\beta\alpha}h_{\beta\alpha s}$) represents heat transfer induced by interphase mass transfer.

CFX uses the Two Resistance Model for interphase heat transfer in conjuction with the intrephase mass transfer. This is achieved by using two heat transfer coefficients ($h_{\alpha,\beta}$) defined on each side of the phase interphase:

$$\frac{1}{h_{\alpha\beta}}=\frac{1}{h_\alpha}+\frac{1}{h_\beta} \tag{7}$$

Thus the interphase mass flux is given by:

$$\dot{m}_{\alpha\beta}=\frac{q_{\alpha\beta}+q_{\beta\alpha}}{H_{\beta s}-H_{\alpha s}} \tag{8}$$

$$q_\alpha=h_\alpha(T_s-T_\alpha) \tag{9}$$
$$q_\beta=h_\beta(T_s-T_\beta)$$

where q_α is the sensible heat flux to phase α from the interface, q_β the sensible heat flux to phase β from the interface and T_s is saturation temperature. $H_{\alpha s}$ and $H_{\beta s}$ represent interfacial values of enthalpy carried into and out of the phases due to phase change. The denominator of Eq. (8) is non-zero, being greater than or equal to the latent heat (L).

Species concentration

$$\frac{\partial}{\partial t}\left(r_\alpha\rho_\alpha Y_{A\alpha}\right)+\nabla\cdot\left(r_\alpha\left(\rho_\alpha\mathbf{U}_\alpha Y_{A\alpha}-\rho_\alpha D_{A\alpha}(\nabla Y_{A\alpha})\right)\right)=\Gamma_\alpha \tag{10}$$

where
$D_{A\alpha}$.... is the kinematic diffusivity
$Y_{A\alpha}$ .... is mass fraction of component A in phase α
Γ... represents interphase mass transfer of component A which is present in two phases.

The interphase species mass transfer is a generalisation of Two Resistance Model previously discussed for heat transfer. Also the interfacial mass flux (m) is expressed in terms of the phasic mass concentations for component n:

$$m_{A\alpha}=-m_{A\beta}=k^{\mathrm{n}}_{\alpha\beta}(K^{\mathrm{n}}\rho_{A\beta}-\rho_{A\alpha}), \tag{11}$$

$$\frac{1}{k^{\mathrm{n}}_{\alpha\beta}}=\frac{1}{k^{n}_{\alpha}}+\frac{K^{\mathrm{n}}}{k^{n}_{\beta}} \tag{12}$$

where
$m_{A\alpha}$ is the mass flux of A to phase α from the interface and $m_{A\beta}$ is the mass flux of A to phase β from the interface. K^n is the mass concentration equilibrium ratio, $\rho_{A\alpha}$ is mass concentration of component A in phase α and $\rho_{A\beta}$ is mass concentration of component A in phase β. In addition, k_β^n and k_α^n are mass transfer coefficients.

The area concentration of the interface $A_{\alpha\beta}$ is modeled by assuming boths phases α and β symmetrically. The surface area per unit volume is calculated from

$$A_{\alpha\beta}=\frac{r_\alpha r_\beta}{d_{\alpha\beta}} \tag{13}$$

where $d_{\alpha\beta}$ is an interfacial length scale.

Assumptions

In stablishing the mathematical model for this process, the following assumptions and simplifications were utilized:

- the flow is laminar and the solid phase is stationary and rigid. This assumption is valid for columnar growth;
- the dissipative interfacial stress is modeled using the mushy zone permeability in analogy with Darcy's law;
- in the phase diagram the liquids solpe (ml) and the partition coefficient (Kn) for component n are assumed to be constants;
- the equilibrium conditions exist at the solid-liquid interface, i.e.

$$T = T_{\mathrm{f}} + \sum_{m} m_{\mathrm{l}} C_{\mathrm{l}}^{\mathrm{n}} \tag{14}$$

and

$$C_{\mathrm{s}}^{\mathrm{n}} = \mathrm{K}^{\mathrm{n}} C_{\mathrm{l}}^{\mathrm{n}} \tag{15}$$

where T_{f} is the fusion temperature, C_{s} is the interface solid concentration and C_{l} is the interface liquid concentration;

- homogeneous and isotropic properties in the phases;
- the liquid within an averaging volume is considered to be solutally well mixed for all species so that the interfacial average and volume average concentrations are equal.

Due to the absence of a general theory or experimental correlations to calculate the phase-diffusion coefficients that appear in the macroscopic conservation equations have been set equal to their microscopic counterparts. Using the preceding approach, no assumptions need to be made regarding whether the rate of mass diffusion of species *n* in the solid if it is fast (i.e., lever rule type behavior) or slow (i.e., Scheil type behavior).

2.2. Numerical procedure

The conservation equations were derived to be valid in the fully solid, mushy, and bulk liquid regions, which allow the computational space to be described on a fixed grid. No interface tracking of the mushy region is needed which further allows the variables to be solved using single-domain numerical procedures.The comercial CFD code CFX-5.7 was used in the current study. A uniform time step of Δt = 3 s was used for sets of simulations. Each time step was converged when the normalized residuals fell below 10^{-6}.The mesh contains 48 994 tetrahedrons elements. The bulk of the geometry contains total number of 9 990 nodes was tested and showed greater refinement.

To test the applicability of the mathematical modelling of fixed thermometric point, a series of problems were investigaded using the present model. The termometer mesures the temperature of the interface near the time scales on these figures begining when the temperature indicated by thermometer was about 692,677 K. Space limitations prohibit the presentation of temperature and concentration plots for all of the elements at each time step. Therefore, representative plots for temperature and selected elements are provided.

3. Results and discussion

The results for case CP Zn are summarized in Fig. 2, it is seen the solidification proceeds from the crucible wall to the center of the ingot. The solutes distribution of Cd, Cu and Fe is shown in Fig. 3. It can be seen that solutes with equilibrium partition ratio K < 1 are preferentially rejected by the freezing interface while with K > 1 are concentrated near the crucible wall in the first frozen solid. The distribution of solute with a low value (Cd, K = 0,02) was similar to that with medium values of K (Fe, K = 0,12).

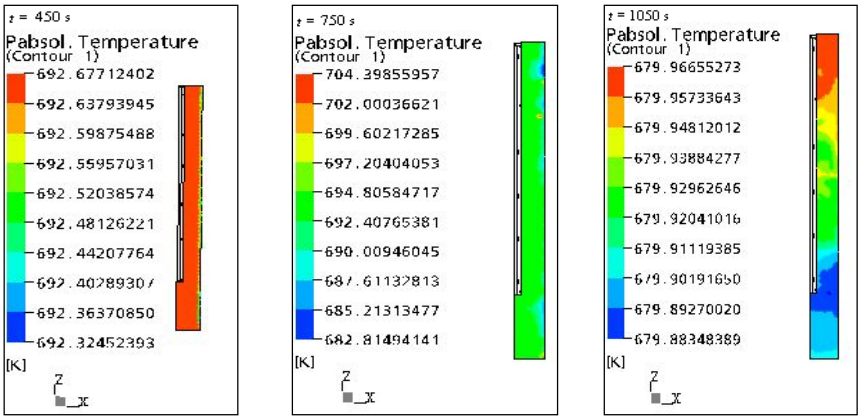

Figure 2.Isotherms and advancement of the solidus front (CP Zn) at times 450 s, 750 s and 1050 s

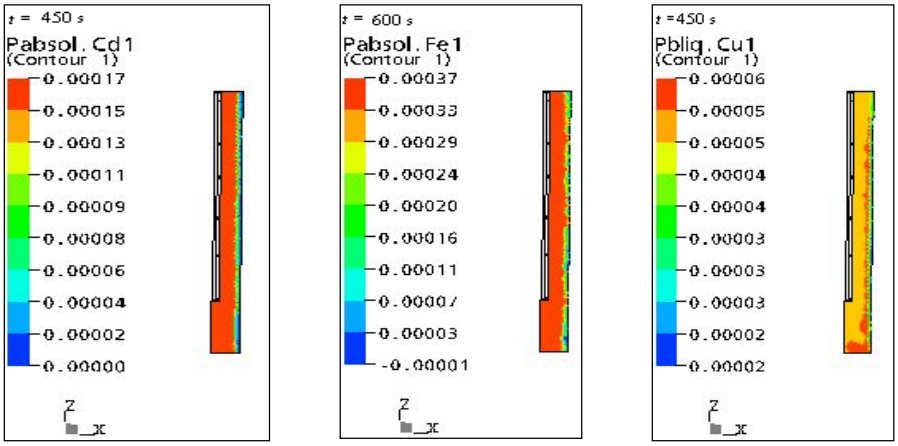

Figure 3. Solute distribution Cd, Fe and Cu in sample CP Zn at times 450 s and 600 s

The results of sample SP Zn is shown in Fig. 4. Comparing these to Fig. 2, it is seen the solidification proceeds from the crucible wall to the center of the ingot. The overall distribution of solute is macroscopically fairly uniform throughout the entire ingot (Fig. 5).

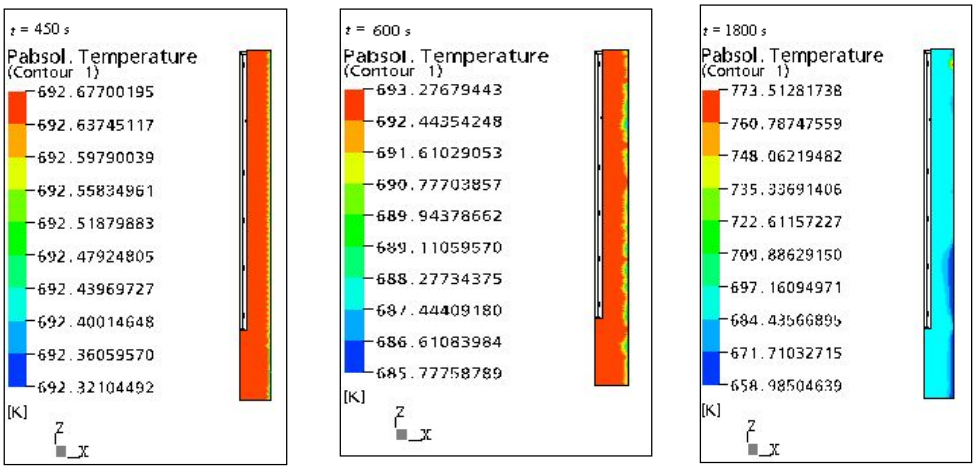

Figure 4. Isotherms and advancement of the solidus front (SP Zn) at times 450 s, 600 s and 1800 s

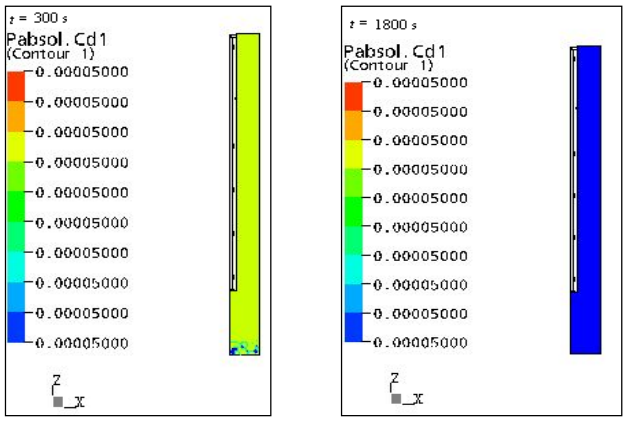

Figure 5. Solute distribution (Cd) of sample SP Zn at times 300 s and 1800 s

For the case of 8 ppm Zn-Tl system (Fig 6) the temperature changes in the melt before transformation occurred under heating rate of 0,02 K/s and after the solidification proceed freely. The results are similar to that SP Zn except for excessive freezing in the higher half of ingot and the outer shell is a little thicker but still relatively uniform. The overall distribution of solute is similar to sample SP Zn (Fig. 5). The same system, at a higher concentration (20 ppm) frozen under heating rate of 0,02 K/s, exhibited similar freezing curves (Fig. 7). For the Zn-Tl system (20 ppm) there was no

essential difference in the solute distribution due to different freezing condition in both cases it is macroscopically uniform throughout the entire ingot.

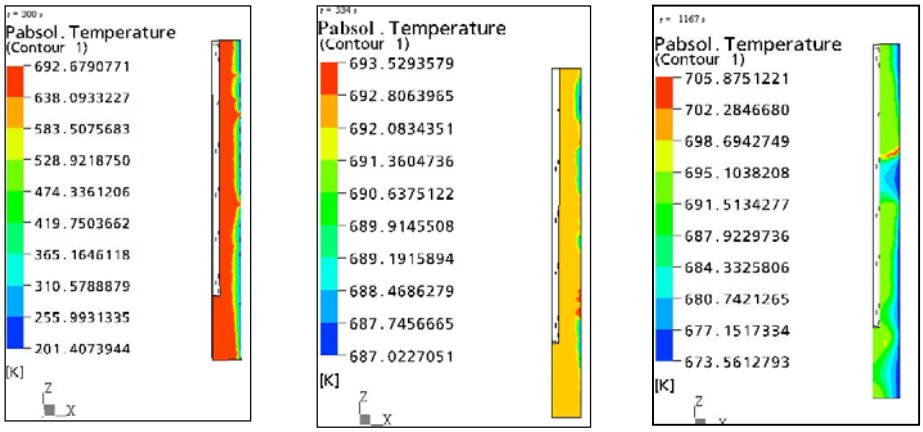

Figure 6. Isotherms and advancement of the solidus front for Zn-Tl system (8 ppm) at times 300 s, 534 s and 1167 s

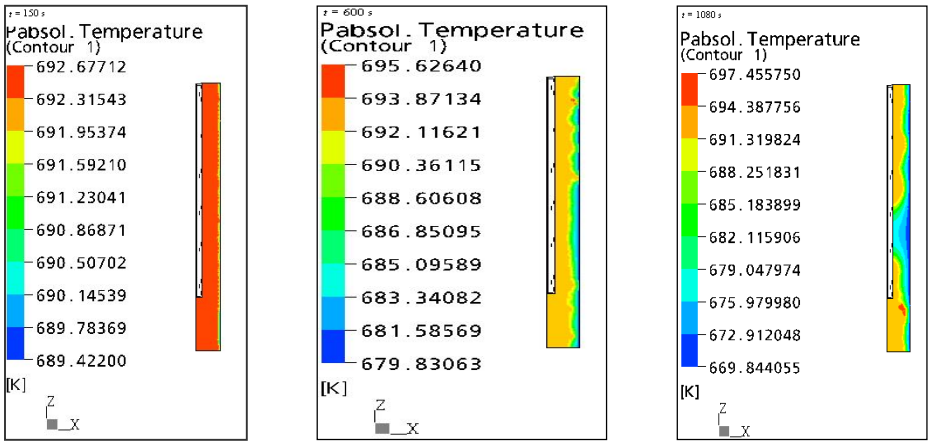

Figure 7. Isotherms and advancement of the solidus front for Zn-Tl system (20 ppm) at times 150 s, 600 s and 1080 s

In general, the solidifications are shorter in time, during about 20 min to 30min.. Estimated depression of the liquidus point from that of the pure element are < 0,02 K for CP Zn, < 0,002 K for SP Zn and Zn-Tl. It were deduced from temperature in the thermometer-well where the sensing element of the thermometer is axially located (x = 4,7mm; y = 0; z = 50 mm). This range of transformation temperature is similar to the results obtained by McLaren (1958) and Weinberg and McLaren (1963). Precise correlation was not possible to achieve because the contents impurities and experimental conditions are not sufficiently well known. In addition, there was a progressive increase for K < 1 (or decrease for K > 1) of solute concentration from the outside to the ingot center. The progressive variation in concentration was most pronounced for the systems containing lower concentration. The convection effects are insiginificant because to the very small temperature gradients in zinc samples. The differences in freezing ranges emphasize the importance of using similar thermal treatments for optimal realization of the defining fixed points of the ITS-90.

5. Conclusions

A two-phase model for continuity, momentum, energy and species transport has been used to simulate the phase changed of zinc freezing point. Although the two phase model has the potential to concurrently resolve many important micro and macro features of alloy solidification, there are many uncertainties involved in the modeling. Major uncertainties relate to the need for a realistic nucleation model, detailed volumetric heat and mass transfer coefficients and correct stereological formations for interfacial area concentration. The complex nature of phase change processes clearly requires considerations which are unique to particular systems. However, the results calculated are in agrement with the published experimental data. Slight differences are noticeable due to the uncertainty of thermophysical

properties used in the current study and the lack of information about experimental conditions. Clearly, there are many other uncertainties associated with inputs to the model (eg., difffusion lenghts and area concentration of the interface) whose importance have not been explored here. The cohesion between the results gives assurance that the current method is numerically accurate in modeling the freezing point. The present results should be viewed as an indication in what subjects require more careful examination if accurate modeling multicomponent solidification is to be accomplished. It is concluded that, the phase transition temperature of a fixed point depend strongly on the experimental conditions, especially impurities concetration.

6. Acknowledgements

It is a pleasure to acknowledge the valuable contribution of Mr. George Bonnier, who suggests this work. This work has been made possible by the Centro de Desenvolvimento de Tecnologia Nuclear - CNEN, for which the authors are grateful.

7. References

BIPM, 1990. "Supplementary information for the international temperature scale of 1990", Bureau International des Poids et Measures, Sèvres, p.177.

BIPM, 1999, On the Influence of Impurities on Fixed-Point Temperatures, Private Communication CCT99-11 of Working Group 1of the CCT.

BIPM,1999, Estimation of Systematic Error due to Impuritiies in Thermometric Fixed Points. Private Communication CCT99-12 of Workin Group 1 of the CCT.

BIPM,2001, PTB Comments on Uncertainty Budgets for Characteristics of SPRTs Calibrated According to the ITS-90, Private Communication, Physikalish-Technische Bundesanstalt, George Bonnier.

Ancsin, J., 2001, "Equilibrium melting curves of relatively pure and doped silver samples", Metrologia, Vol.380, pp. 229-235.

Ancsin, J., 2003, "Impurity dependence of the aluminium point", Metrologia, Vol.40, pp. 36-41.

Brady, G.S. and Clauses H.R, 1991, "Materials Handbook", 13nd Edition, McGraw-Hill, Inc.

Campos, M.P.F and Davies, G.J., 1978, "Solidificação e Fundação de Metais e suas Ligas", Ed. da Universidade de São Paulo, S.Paulo, Brazil, 246 p.

Connolly, J.J. and McAllan, J.V., 1980, "Limitations on Metal Fixed Points Caused by Trace Impurities", Metrologia, Vol. 16, pp. 127-132.

Connolly, J.J. and McAllan, J.V., 1975, "The Tin-Iron Eutectic", Acta Metallurgica,Vol.23,pp. 1209-1214.

Ilegbusi, O.J. and Nat, M.D., 2000,"A Review of the Modeling of Multi-Phase Phenomena in Materials Processing-I.Solid-Liquid Systems", Journal of Materials Processing & Manufacturing Science, Vol.8,pp. 188-217.

ILZR, 1991, "Zinc Handbook. Properties, Processing and Use in Design", International Lead Zinc Research Organization, Inc., Research Triangle Park, North Carolina. Franck C. Porter, Dekker Inc., New York.

McLaren, E.G.,1958, "The Freezing Points of High Purity Metals as Precision Temperature Standards. III Thermal Analyses on Eight Grades of Zinc with Purities Greater than 99,99+%", Can. J. Phys.,Vol.36, pp.585-598.

McLaren, E.G.,1962, "The Freezing Points of High Purity Metals as Precision Temperature Standards", Temperature-Its Measuremet and Control in Science and Industry, Vol. 3, Part 1, pp.185-198.

McLaren, E.G.,1963, "The Freezing Points of High Purity Metals as Precision Temperature Standards.VII. Thermal Analyses on Seven Samples of Bismuth with Purities Greater Than 99,999+%", Can. J. Phys.,Vol.41, pp.95-111.

Ni, J. and Beckermann, C., 1991, "A Volume-averaged Two-phase Model for Transport Phenomena During Solidification", Metal. Trans. B., Vol. 22B,pp. 349-361.

Sostmann, H. and Tavener, J.P, 1993, "Fundamentals of Thermometry Part VII Metal Melting and Freezing Equilibria Phase, Phase diagrams, Cryoscopic Constant". Isotech Journal of Thermometry, Vol.4,No.1, pp.59-80.

Sostmann, H., 1993, "Fundamentals of Thermometry Part II Fixed Points of the ITS-90". Isotech Journal of Thermometry, Vol.4,No.2, pp.49-78.

Weinberg, F. and McLaren, E.H., 1963 "The solidfication of Dilute Binary Alloys", Transactions of the metallurgical Society of AIME, Vol.227, pp. 112-124.

8. Responsibility notice

The authors Denise das M. Camarano, Vinícius S. Moreira and Roberto M. de Andrade are the only responsible for the printed material included in this paper.